LETTER

doi:10.1038/nature10935

A close halo of large transparent grains around extreme red giant stars

Barnaby R. M. Norris[1], Peter G. Tuthill[1], Michael J. Ireland[1,2,3], Sylvestre Lacour[4], Albert A. Zijlstra[5], Foteini Lykou[5], Thomas M. Evans[1,6], Paul Stewart[1] & Timothy R. Bedding[1]

An intermediate-mass star ends its life by ejecting the bulk of its envelope in a slow, dense wind[1–3]. Stellar pulsations are thought to elevate gas to an altitude cool enough for the condensation of dust[1], which is then accelerated by radiation pressure, entraining the gas and driving the wind[2,4,5]. Explaining the amount of mass loss, however, has been a problem because of the difficulty of observing tenuous gas and dust only tens of milliarcseconds from the star. For this reason, there is no consensus on the way sufficient momentum is transferred from the light from the star to the outflow. Here we report spatially resolved, multiwavelength observations of circumstellar dust shells of three stars on the asymptotic giant branch of the Hertzsprung–Russell diagram. When imaged in scattered light, dust shells were found at remarkably small radii (less than about two stellar radii) and with unexpectedly large grains (about 300 nanometres in radius). This proximity to the photosphere argues for dust species that are transparent to the light from the star and, therefore, resistant to sublimation by the intense radiation field. Although transparency usually implies insufficient radiative pressure to drive a wind[6,7], the radiation field can accelerate these large grains through photon scattering rather than absorption[8]—a plausible mass loss mechanism for lower-amplitude pulsating stars.

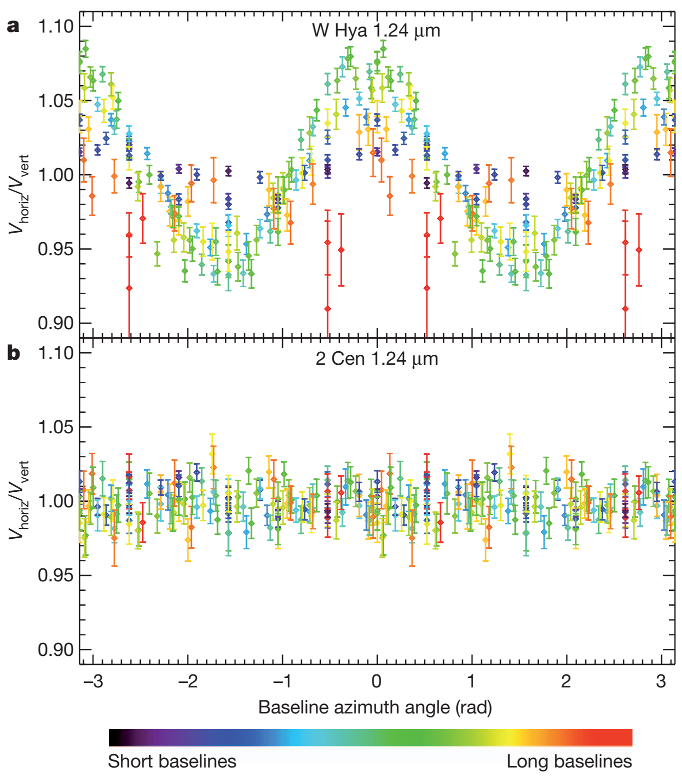

Figure 1 | Polarimetric interferometry of W Hya at 1.24 μm. Although light scattered by each part of the circumstellar dust shell is strongly polarized, the integrated signal recovered with conventional polarimetry is zero for an unresolved spherically symmetric shell. In this study, aperture-masking interferometry[9,10] (which converts the 8-m pupil of the Very Large Telescope into a multi-element interferometer, using the NACO[24] instrument) allows access to the ~10-mas spatial scales required to resolve the shell, and polarimetric measurements (obtained by simultaneously measuring interferometric visibilities in orthogonal polarizations[25]) allows light from the star and light from the dust shell to be differentiated. Here the ratio of the horizontally polarized visibilities (V_{horiz}) to vertically polarized visibilities (V_{vert}) is plotted against baseline azimuth angle (corresponding to position angle on the sky). Colour encodes the baseline length (longest, 7.3 m; shortest, 0.56 m). The ratio V_{horiz}/V_{vert} is a differential observable, which allows the cancellation of residual systematic errors and depends only on the fractional polarized scattered light signal. **a**, Result for W Hya, an AGB star with a circumstellar shell; V_{horiz}/V_{vert} deviates from 1, varying sinusoidally with azimuth. This is the signal expected from a thin, spherically symmetric dust shell scattering the light from a central star. This signal varies in amplitude for different baselines, encoding the spatial extent of the resolved structure. Data points have been repeated over two cycles. The longest baselines (red) have poor signal-to-noise ratios because they are close to the null, where the visibility curve of the star is extremely low. Error, 1σ. **b**, Visibility data for the star 2 Cen, which has no circumstellar dust shell and, hence, no polarized signal from scattering; here $V_{horiz}/V_{vert} \approx 1$ for all azimuths. Errors, 1σ.

We observed W Hydrae, R Doradus and R Leonis using aperture-masked[9,10] polarimetric interferometry (Fig. 1), along with dust-free stars to verify our detection methodology. Figure 1 shows the ratio of the horizontally and vertically polarized visibilities (V_{horiz}/V_{vert}), plotted as a function of baseline azimuth and length. The dust-free star 2 Centauri, which has no polarized flux, shows a constant ratio $V_{horiz}/V_{vert} = 1.0$ within its uncertainties. However, the dust-enshrouded star W Hya shows a strong sinusoidal variation of V_{horiz}/V_{vert} with azimuth, as expected from a resolved circumstellar scattering shell. By taking advantage of spherical symmetry, we produced the much simpler baseline-dependent observable plotted in Fig. 2. A model was then fitted to the data to determine the dust shell radius and the amount of light scattered by the shell at each wavelength (Supplementary Information). These results are summarized in Table 1. Figure 3 shows the model image of the star and shell as seen in orthogonal polarizations for W Hya at a wavelength of 1.24 μm, from which the model visibilities were derived.

Scattered-light dust shells around the three asymptotic giant branch (AGB) stars observed were found close to the star, at radii $\lesssim 2$ stellar radii. This is in contrast to earlier models that place the shell at many stellar radii[2], but is consistent with some recent models[6] and with interferometric[11] and polarimetric[12] measurements. On the basis of typical elemental abundances and spectral observations, the composition of

[1]Sydney Institute for Astronomy, School of Physics, University of Sydney, New South Wales 2006, Australia. [2]Department of Physics and Astronomy, Macquarie University, New South Wales 2109, Australia. [3]Australian Astronomical Observatory, PO Box 296, Epping, New South Wales 1710, Australia. [4]LESIA-Observatoire de Paris, CNRS, Université Pierre et Marie Curie, Université Paris-Diderot, Meudon 92190, France. [5]Jodrell Bank Centre for Astrophysics, School of Physics & Astronomy, University of Manchester, Oxford Road, Manchester M13 9PL, UK. [6]Department of Physics, Denys Wilkinson Building, Keble Road, University of Oxford, Oxford OX1 3RH, UK.

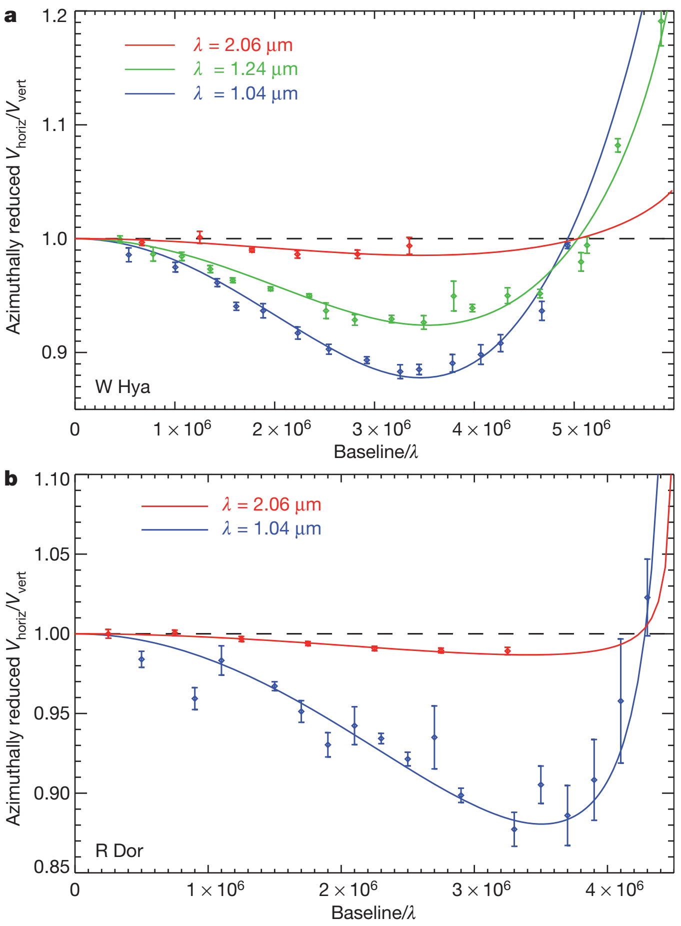

Figure 2 | Wavelength dependence of scattering for W Hya and R Dor. The azimuthally reduced ratio V_{horiz}/V_{vert} for the AGB stars W Hya and R Dor, plotted against spatial frequency (baseline length divided by wavelength, λ), at multiple wavelengths. The functional form of the visibility ratio excursions of all three AGB stars are consistent, within uncertainties, with a simple spherically symmetric shell. We were therefore able to enhance our signal-to-noise ratio significantly in a quantitative analysis by reducing our two-dimensional visibility data to a one-dimensional function of the baseline length (corresponding to spatial frequency). This was achieved by dividing V_{horiz}/V_{vert} by the expected sinusoidal variation (characteristic of a spherical shell) at a fixed amplitude, resulting in the much simpler, baseline-dependent observable plotted here. Points are the observed data (binned; errors, 1σ) and the solid lines are the fitted model. The spatial frequency of the minimum of the characteristic 'dip' varies with the radius of the dust shell: for a larger shell, the minimum of the dip occurs at lower spatial frequencies. The depth of the dip depends on the amount of scattered light, with a larger deviation from $V_{horiz}/V_{vert} = 1.0$ indicating that a larger fraction of the total flux arises from light scattered by the shell. This is seen to decrease strongly at longer wavelengths as expected theoretically; the precise change in this quantity as a function of wavelength can be used to determine the dust grain radius using Mie scattering theory (Fig. 4). The fitted parameters for these quantities are included in Table 1. The 2.06-μm data have insufficient spatial resolution to constrain the shell size, so for models at these wavelengths we fixed the shell size to be consistent with the fitted size at shorter wavelengths.

AGB dust shells is expected to be dominated by silicates[5,13,14] in the form of olivine ($Mg_{2x}Fe_{2(1-x)}SiO_4$) and/or pyroxene ($Mg_xFe_{(1-x)}SiO_3$), where $0 \leq x \leq 1$. The temperature of a grain is determined by its opacity, that is, how strongly it absorbs the surrounding radiation field. Multiwavelength models[6] show that silicate dust that contains iron absorbs the stellar flux strongly (as these dust species have high opacities at wavelengths of ~1 μm, where the energy distribution peaks) and so can only condense at distances greater than ~5 stellar radii. These iron-rich species could be accelerated by absorption of stellar radiation, but they form too far from the star to provide an efficient mass loss mechanism for low-amplitude pulsators[6] (semiregular variable stars). Our detection of dust much closer to the star is instead consistent with the presence of iron-free silicates such as forsterite (Mg_2SiO_4) and enstatite ($MgSiO_3$), which are almost transparent at wavelengths of ~1 μm. Such grains do not heat to sublimation, despite the intense radiation close to the star, but the same transparency also prevents the momentum transfer from starlight required to drive a wind. For some stars, a possible solution to this dilemma arises when very large grains are considered.

The degree of scattering by dust depends strongly on the wavelength of the incident light and on the size of the particles. By analysing our multiwavelength measurements using Mie scattering theory, we determined the effective grain size and the number of grains. As shown in Fig. 4, we found an effective grain radius of ~300 nm. For grains of this size, the scattering opacity becomes very large, well beyond that resulting from Rayleigh scattering when the particles are smaller. In this regime, the contribution to radiative acceleration by scattering, rather than by absorption alone, must be considered. Models show that grains exceeding a certain critical scattering opacity can drive a wind at high magnesium condensation and that, for a star of temperature 2,700 K, this critical scattering opacity is only exceeded in a narrow range of dust grain radii around 300 nm (ref. 8). We also note that a narrow range of grain radii, of the order of ~500 nm, is predicted on the basis of a self-regulating feedback mechanism: grain growth effectively halts once the critical size is reached, because the dust is then accelerated outwards and gas densities quickly decrease[8]. This is consistent with observations of grains in the interstellar medium, which are dominated by silicates[15] and have similar grain sizes[16,17]. Wind driving due to scattering by magnesium-rich silicates is consistent with the finding that mass loss in AGB stars depends on their metallicity[18]. Although this model encounters difficulties in the case of stars with extremely extended atmospheres, such as R Leo (owing to the mass of the stellar atmosphere at and above the dust-forming layers being too high to allow sufficient acceleration[19]), it provides a plausible explanation for the mass loss of semiregular pulsating stars such as R Dor. Our

Table 1 | Summary of fitted model parameters

Star	Φ	λ (μm)	R_{star} (mas)	R_{shell} (mas)	Scattered fraction	Grain radius (nm)	Scattering-shell mass
R Dor	0.7	1.04	27.2 ± 0.2	43.3 ± 0.3	0.124 ± 0.003	299 ± 39	$(2.7 \pm 0.2) \times 10^{-10} M_\odot$
		2.06	27.7 ± 1.4	43.6 ± 3.2	0.014 ± 0.002		
W Hya	0.2	1.04	18.7 ± 0.4	37.9 ± 0.2	0.176 ± 0.002	316 ± 4	$(1.04 \pm 0.02) \times 10^{-9} M_\odot$
		1.24	18.9 ± 0.5	37.0 ± 0.3	0.110 ± 0.003		
		2.06	18.9 (fixed)	37.0 (fixed)	0.022 ± 0.004		
R Leo	0.4	1.04	18.3 ± 0.3	29.9 ± 0.4	0.120 ± 0.003	~300*	$\sim 2 \times 10^{-10} M_\odot$

The radii of the dust shells were found to be $\lesssim 2R_{star}$. The scattered fraction is the proportion of the total flux arising from scattering by the dust shell. The grain radius was obtained from fitting to multiwavelength observations using Mie scattering (with the value for R Leo fixed at 300 nm). The scattering-shell mass was calculated only for the observed dust (and not, for example, for a distribution extending to small grains invisible to our technique). Stellar radii given are for a uniform disc. All three AGB stars (W Hya, R Dor and R Leo) were observed in March 2009, with additional observations of W Hya at 1.24 μm and 2.06 μm made in June 2010. Although the photospheric diameter, and possibly the dust shell diameter, are expected to vary throughout the stellar pulsation cycle, the two sets of observations for W Hya were taken approximately one period apart and have therefore been combined. These figures assume both the dust to be iron-free silicate (forsterite) grains of uniform size and there to be full magnesium condensation. Full magnesium condensation is a reasonable assumption for the stars with more compact atmospheres (for example R Dor) but is inconsistent with observed optical depths for stars with more extended atmospheres[19]. In the event that there is also a population of small, weakly scattering grains that do not show up in our data, these values represent lower limits, with the total shell mass being greater. Furthermore, if the shell is geometrically extended then the true mass will be greater, as these calculations assume a thin shell. The uncertainties given are based on random errors and do not account for systematic errors such as those described here. Hipparcos parallaxes[22] and experimentally measured optical constants[23] have been used. Φ indicates visual phase, derived from the AAVSO International Database; R_{star}, stellar radius; R_{shell}, radius of dust shell.

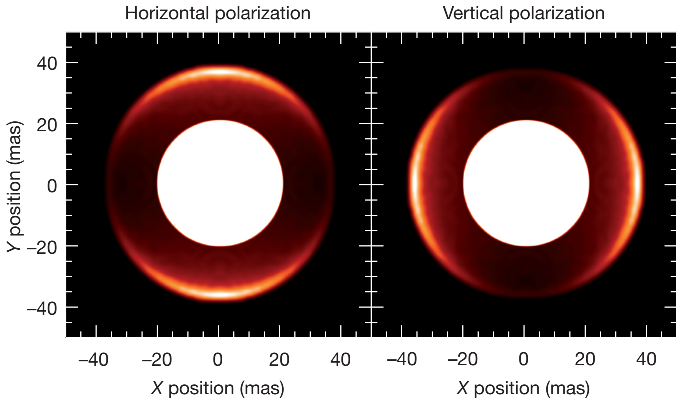

Figure 3 | Model image for W Hya with circumstellar shell viewed in horizontally and vertically polarized light. The white disc represents the uniform-disc star used in the model. A three-dimensional model of a star with a thin scattering shell was constructed, and the scattered intensity observed in each polarization for each point on the shell was calculated using Mie scattering, yielding an image of the star and shell. We then derived polarized visibilities from the model and fitted them to the observed visibilities, to determine the dust shell radius and the scattered fraction. Details of the modelling process can be found in Supplementary Information. See Supplementary Fig. 2 for a diagram illustrating how the polarized intensity distribution arises.

observations provide direct evidence for a population of dust grains capable of powering a scattering-driven wind.

The last column of Table 1 gives the mass of the dust that contributes to the observed scattering signal, assuming the shell to be thin and the dust grains to be forsterite of a uniform size. If full magnesium condensation and solar abundances are assumed, then the gas-to-dust ratio is ~600, which yields total shell masses of $\sim 6 \times 10^{-7} M_\odot$, $\sim 2 \times 10^{-7} M_\odot$ and $\sim 1 \times 10^{-7} M_\odot$ for W Hya, R Dor and R Leo, respectively. Because the pulsation periods of these stars are ~1 yr and the mass loss rates are $\sim 1 \times 10^{-7} M_\odot \,\mathrm{yr}^{-1}$ (refs 20, 21), this implies that for stars with less extended atmospheres a large fraction of the observed shell is ejected each pulsation cycle, consistent with the observed dust being part of an outflow. In the extended-atmosphere case, where full magnesium condensation is not observationally supported, a possible alternative dust species is corundum (Al_2O_3),

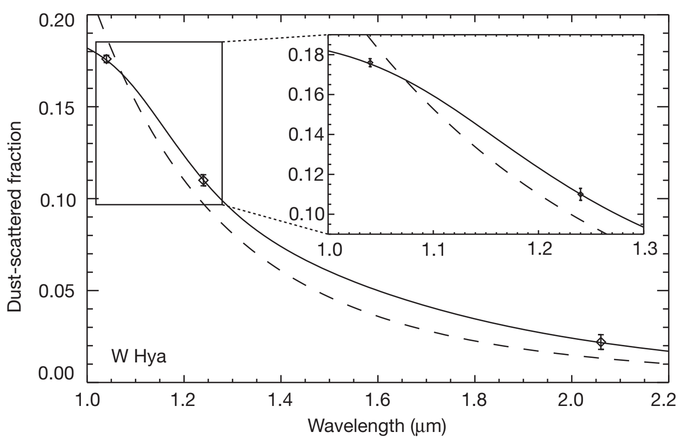

Figure 4 | Grain size measurement. Grain size fitted to the fraction of scattered light as a function of wavelength, for W Hya. Inset, magnified view of the 1.0–1.3-μm region. The solid line represents the fitted Mie scattering model (where grain size and grain number were fit parameters), and the dashed line represents the best Rayleigh fit (where grain size was fixed to be below the Rayleigh limit). The data are inconsistent with Rayleigh scattering. The fitted Mie model yields an effective grain radius of 316 ± 4 nm. In reality, a distribution of grain sizes may be present; for example, a population of very much smaller particles would contribute only weakly and could be undetected. Our data show that, regardless of the presence or absence of smaller grains, a population of large, ~300-nm, grains is required. Errors, 1σ.

as discussed in Supplementary Information. Further time-dependent grain growth and dynamical models will help elucidate the role of light scattered from large-grained dust in the process of mass loss from AGB stars.

Received 25 October 2011; accepted 9 February 2012.

1. Wood, P. R. Pulsation and mass loss in Mira variables. *Astrophys. J.* **227,** 220–231 (1979).
2. Habing, H. J. Circumstellar envelopes and asymptotic giant branch stars. *Astron. Astrophys. Rev.* **7,** 97–207 (1996).
3. Marengo, M. A review of AGB mass loss imaging techniques. *Proc. Astron. Soc. Aust.* **26,** 365–371 (2009).
4. Gustafsson, B. & Höfner, S. *Asymptotic Giant Branch Stars* (eds Habing, H. J. & Olofsson, H.) Ch. 4 (Springer, 2004).
5. Höfner, S. Dust formation and winds around evolved stars: the good, the bad and the ugly cases. *Astron. Soc. Pacif. Conf. Ser.* **414,** 3–21 (2009).
6. Woitke, P. Too little radiation pressure on dust in the winds of oxygen-rich AGB stars. *Astron. Astrophys.* **460,** L9–L12 (2006).
7. Ireland, M. J. & Scholz, M. Observable effects of dust formation in dynamic atmospheres of M-type Mira variables. *Mon. Not. R. Astron. Soc.* **367,** 1585–1593 (2006).
8. Höfner, S. Winds of M-type AGB stars driven by micron-sized grains. *Astron. Astrophys.* **491,** L1–L4 (2008).
9. Tuthill, P. G., Monnier, J. D., Danchi, W. C., Wishnow, E. H. & Haniff, C. A. Michelson interferometry with the Keck I Telescope. *Publ. Astron. Soc. Pacif.* **112,** 555–565 (2000).
10. Lacour, S. *et al.* Sparse aperture masking at the VLT. I. Faint companion detection limits for the two debris disk stars HD 92945 and HD 141569. *Astron. Astrophys.* **532,** A72 (2011).
11. Wittkowski, M. *et al.* The extended atmospheres of Mira variables probed by VLTI, VLBA, and APEX. *Astron. Soc. Pacif. Conf. Ser.* **445,** 107–112 (2011).
12. Ireland, M. J., Tuthill, P. G., Davis, J. & Tango, W. Dust scattering in the Miras R Car and RR Sco resolved by optical interferometric polarimetry. *Mon. Not. R. Astron. Soc.* **361,** 337–344 (2005).
13. Waters, L. B. F. M. *et al.* Mineralogy of oxygen-rich dust shells. *Astron. Astrophys.* **315,** L361–L364 (1996).
14. Gail, H.-P. in *Astromineralogy* (ed Henning, T. K.) 55–120 (Lect. Notes Phys. 609, Springer, 2003).
15. Draine, B. T. Interstellar dust grains. *Annu. Rev. Astron. Astrophys.* **41,** 241–289 (2003).
16. Frisch, P. C. *et al.* Dust in the local interstellar wind. *Astrophys. J.* **525,** 492–516 (1999).
17. Weingartner, J. C. & Draine, B. T. Dust grain-size distributions and extinction in the Milky Way, Large Magellanic Cloud, and Small Magellanic Cloud. *Astrophys. J.* **548,** 296–309 (2001).
18. Lagadec, E. & Zijlstra, A. A. The trigger of the asymptotic giant branch superwind: the importance of carbon. *Mon. Not. R. Astron. Soc.* **390,** L59–L63 (2008).
19. Ireland, M. J., Scholz, M. & Wood, P. R. Dynamical opacity-sampling models of Mira variables - II. Time-dependent atmospheric structure and observable properties of four M-type model series. *Mon. Not. R. Astron. Soc.* **418,** 114–128 (2011).
20. Loup, C., Forveille, T., Omont, A. & Paul, J. F. CO and HCN observations of circumstellar envelopes. A catalogue—mass loss rates and distributions. *Astron. Astrophys. Suppl. Ser.* **99,** 291–377 (1993).
21. Olofsson, H., González Delgado, D., Kerschbaum, F. & Schöier, F. L. Mass loss rates of a sample of irregular and semiregular M-type AGB-variables. *Astron. Astrophys.* **391,** 1053–1067 (2002).
22. van Leeuwen, F. Validation of the new Hipparcos reduction. *Astron. Astrophys.* **474,** 653–664 (2007).
23. Jäger, C., Dorschner, J., Mutschke, H., Posch, T. & Henning, T. Steps toward interstellar silicate mineralogy. VII. Spectral properties and crystallization behaviour of magnesium silicates produced by the sol-gel method. *Astron. Astrophys.* **408,** 193–204 (2003).
24. Lenzen, R. *et al.* NAOS-CONICA first on sky results in a variety of observing modes. *Proc. SPIE* **4841,** 944–952 (2003).
25. Tuthill, P. *et al.* Sparse aperture masking (SAM) at NAOS/CONICA on the VLT. *Proc. SPIE* **7735,** 773510 (2010).

Supplementary Information is linked to the online version of the paper at www.nature.com/nature.

Acknowledgements This work was based on observations collected with the NACO instrument at the European Southern Observatory, Chile.

Author Contributions P.G.T., M.J.I. and S.L. commissioned the SAMPol observing mode and conducted the initial observations, and developed the standard aperture-masking data reduction pipeline. B.R.M.N. developed the polarimetric data reduction and modelling/fitting procedures, analysed the data and conducted later observations. T.M.E. and P.S. contributed to the data analysis procedures. T.R.B., A.A.Z. and F.L. contributed to both the observing programme and the interpretation of the findings.

Author Information Reprints and permissions information is available at www.nature.com/reprints. The authors declare no competing financial interests. Readers are welcome to comment on the online version of this article at www.nature.com/nature. Correspondence and requests for materials should be addressed to B.R.M.N. (bnorris@physics.usyd.edu.au).